EUROPHYSICS LETTERS 15 June 2005

Europhys. Lett., **70** (6), pp. 836–842 (2005)
DOI: 10.1209/epl/i2005-10039-9

Formation of nanoscale pore arrays during anodization of aluminum

G. K. Singh[1], A. A. Golovin[1], I. S. Aranson[2] and V. M. Vinokur[2]

[1] *Department of Engineering Sciences and Applied Mathematics Northwestern University - Evanston, IL 60208, USA*
[2] *Materials Science Division, Argonne National Laboratory 9700 S. Cass Ave., Argonne, IL 60439, USA*

received 1 March 2005; accepted in final form 18 April 2005
published online 11 May 2005

PACS. 82.45.Cc – Anodic films.
PACS. 82.45.Yz – Nanostructured materials in electrochemistry.
PACS. 89.75.Kd – Patterns.

Abstract. – A theory of the spontaneous formation of spatially regular hexagonal arrays of nanopores in aluminum oxide film growing during aluminum anodization is presented. Linear stability analysis shows that, in certain ranges of the applied voltage and electrolyte *p*H, the oxide film is unstable with respect to perturbations with a well-defined wavelength. The instability is caused by a positive feedback between the oxidation-dissolution rates and variations of electric field caused by perturbations of the metal-oxide and oxide-electrolyte interfaces. The competition between this instability and the stabilizing effects of the Laplace pressure and elastic stress provides the wavelength selection mechanism. The hexagonal ordering of pores results from the resonant quadratic nonlinear interaction of unstable modes.

Spatially regular, hexagonally ordered arrays of nanoscale pores in aluminum oxide can be formed by the anodization of aluminum in acidic electrolytes [1–3]. Nanoporous alumina has attracted renewed attention lately as a promising material for the fabrication of new magnetic storage devices, catalytic membranes, and as an inexpensive template for the production of nanoscale particles, wires, and photonic crystals [4].

Despite many experimental studies and general understanding of the pore growth mechanism to be associated with electric-field–assisted dissolution of aluminum oxide, the mechanism of *self-organization* of regular pore arrays is not understood. A model for the steady growth of a single pore, based on the field-assisted dissolution, was proposed in [5]. A similar model was considered in [6] and a long-wave linear stability analysis of the interfaces was performed. It can be shown, however, that the model studied in [6] does not provide a physically justified short-wave cutoff and hence a regularization mechanism needs to be identified that would explain the selection of the pore diameter and interpore spacing. One such mechanism is the dependence of the activation energies of the interfacial reactions on the Laplace pressure at the curved interfaces due to surface energy [7]. An additional important factor may be the elastic stress caused by the volume expansion in the course of the $Al \rightarrow Al_2O_3$ reaction [8]. The presence of elastic stress can significantly affect the morphological stability of the surface [9].

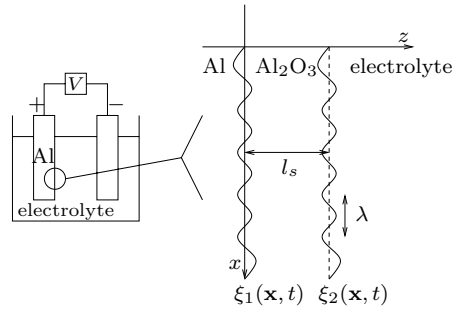

Fig. 1 – Interfaces at the aluminum anode.

In this letter, we propose a theory for the formation of regular and irregular arrays of nanopores in aluminum oxide during the anodization of aluminum. We show that a nonlinear dependence of the surface current on the overpotential and a dependence of the activation energies on the Laplace pressure and elastic stress can explain the formation of both irregular and hexagonally ordered pore arrays.

Consider an electrolytic cell with an aluminum anode and acidic electrolyte. A constant voltage V is applied across the cell and the resulting electrochemical reaction creates a layer of aluminum oxide on the surface of the aluminum electrode. It is generally accepted that, once formed, the oxide layer grows due to the oxidation reaction sustained by the electromigration of oxygen and hydroxyl ions through the existing layer to the metal-oxide interface [10]. At the same time, dissolution of the oxide occurs at the oxide-electrolyte interface.

The positions of the metal-oxide and oxide-electrolyte interfaces are represented by $\xi_1(\boldsymbol{x}, t)$ and $\xi_2(\boldsymbol{x}, t)$, respectively, as shown schematically in fig. 1. Since the conductivities of the aluminum and electrolyte are much larger than that of the oxide, we assume the main part of the voltage drop to occur in the oxide layer. We assume also that the conductivity of the oxide is constant and therefore the conservation of charge there is described by the Laplace equation for the electric potential $\varphi(\boldsymbol{x}, z, t)$. The potential from the metal side of the metal-oxide interface is fixed at V, and the potential from the electrolyte side of the oxide-electrolyte interface is fixed at zero. We neglect the perturbation of the electric field due to ion migration as well as the effect of the electric double layer at the metal-oxide interface. At the oxide-electrolyte interface, however, the double layer induces a jump in the potential across the interface. The electric current across the interface (sustained by oxygen or hydroxyl ions produced in interfacial reactions) depends exponentially on this potential jump, as prescribed by the Butler-Volmer relation [11]. Thus, the dynamics of the metal-oxide and oxide-electrolyte interfaces can be described as follows:

$$\nabla^2\varphi = 0, \qquad \xi_1(\boldsymbol{x}, t) < z < \xi_2(\boldsymbol{x}, t); \tag{1}$$

$$z = \xi_1 : \qquad \varphi = V, \tag{2}$$

$$v_n^{(1)} = a\sigma\partial_n\varphi; \tag{3}$$

$$z = \xi_2 : \qquad -\sigma\partial_n\varphi = k_+ e^{\alpha\varphi} - k_- e^{-\alpha\varphi}, \tag{4}$$

$$v_n^{(2)} = -b_+ k_+ e^{\alpha\varphi} + b_- k_- e^{-\alpha\varphi}. \tag{5}$$

Here $v_n^{(1,2)}$ are the normal velocities of the metal-oxide and oxide-electrolyte interfaces, σ is the conductivity of the oxide, $k_\pm$ are kinetic coefficients characterizing the interfacial current of oxygen or hydroxyl ions produced in the oxide dissolution reaction at the oxide-electrolyte

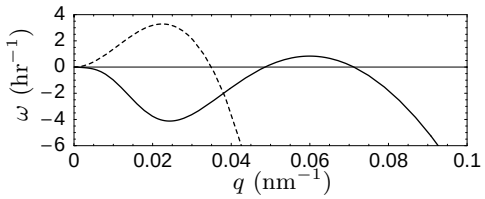

Fig. 2 – Typical dispersion curves showing the unstable modes in the absence (dashed line) and in the presence (solid line) of the elastic stress. The parameters for both lines are the same (see text), except that for the dashed line, $s_{ij}^{\pm} = 0$, $\gamma^{+} = -10.94\,\mathrm{N\,m^{-1}}$, and $\gamma^{-} = 7.29\,\mathrm{N\,m^{-1}}$.

interface, and a and $b_{\pm}$ are Faradaic coefficients relating the rate of the interface motion to the interfacial current. The constant $\alpha = q_e/(2k_BT)$, where q_e is the electron charge, k_B is the Boltzmann constant, T is the absolute temperature, and $1/2$ is the symmetry factor, assumed equal for the forward and reverse reactions [11]. The activation energies of the oxide-electrolyte interfacial reactions depend on the Laplace pressure and elastic stress,

$$k_{\pm} = k_{\pm}^{\circ} \exp\left[\frac{1}{\rho k_B T}\left(\gamma^{\pm}\kappa + s_{ij}^{\pm}\sigma_{ij}\right)\right], \tag{6}$$

where ρ is the number density of the oxide, κ is the curvature of the interface, and σ_{ij} is the stress tensor evaluated at the oxide-electrolyte interface. The activation surface energies (activation energy per unit area) $\gamma^{\pm} = \rho(\partial E_a^{\pm}/\partial\kappa)$, where $E_a^{\pm}$ are the activation energies of the forward (+) and reverse (−) reactions, $\gamma^{+} < 0$, $\gamma^{-} > 0$. Similarly, the activation strains, $s_{ij}^{\pm} = \rho(\partial E_a^{\pm}/\partial\sigma_{ij})$, measure the dependence of the activation energies on the elastic stresses [9]. The "chemical" factor of the oxide dissolution rate, k_{+}°, depends on the pH, $k_{+}^{\circ} = \bar{k}_{+}^{\circ} 10^{-p\mathrm{H}}$ [5].

Consider the growth of a planar oxide layer with thickness $l(t) = \xi_2(t) - \xi_1(t)$. The solution of (1) for planar interfaces is $\varphi_0(t) = V - E(t)[z - \xi_1(t)]$, where $E(t)$ is the electric field. The boundary conditions (2)-(5) give a system of equations for E and l,

$$\begin{aligned} \sigma E &= k_{+}e^{\alpha(V-El)} - k_{-}e^{-\alpha(V-El)}, \\ \frac{\mathrm{d}l}{\mathrm{d}t} &= a\sigma E - b_{+}k_{+}e^{\alpha(V-El)} + b_{-}k_{-}e^{-\alpha(V-El)}. \end{aligned}$$

This system has the stationary solution

$$E_s = \sigma^{-1}\sqrt{k_{+}k_{-}}(r - r^{-1}), \qquad r = \sqrt{\frac{a - b_{-}}{a - b_{+}}}, \tag{7}$$

$$l_s = \frac{\sigma}{\sqrt{k_{+}k_{-}}} \frac{V - \alpha^{-1}\ln(r\sqrt{k_{-}/k_{+}})}{r - r^{-1}}. \tag{8}$$

The solution (7)-(8) exists only for real $r > 1$ and describes a planar oxide layer uniformly propagating with velocity $v_s = -a\sigma E_s$; we consider it as the *basic state*. For typical parameter values [1, 3, 10]: $V = 50\,\mathrm{V}$, $\alpha = 15.56\,\mathrm{V^{-1}}$, $\sigma = 5 \times 10^{-9}\,\mathrm{A\,m^{-1}\,V^{-1}}$, $\bar{k}_{+}^{\circ} = k_{-}^{\circ} = 20\,\mathrm{A\,m^{-2}}$, $p\mathrm{H} = 0$, $a = 1.04 \times 10^{-10}\,\mathrm{m^3\,C^{-1}}$, $b_{+} = 5.18 \times 10^{-11}\,\mathrm{m^3\,C^{-1}}$, $b_{-} = 2.59 \times 10^{-11}\,\mathrm{m^3\,C^{-1}}$, $s_{ij}^{\pm} = 0$, one obtains $l_s = 30\,\mathrm{nm}$ and $v_s = -1\,\mathrm{nm\,s^{-1}}$.

We now study the stability of the oxide layer in the basic state. First, consider the case when the activation energies of the interfacial reactions do not depend on stress, *i.e.* we set

$s_{ij}^{\pm} = 0$ in (6). For infinitesimal perturbations of the basic state solution, $\mathcal{G} - \mathcal{G}_0 = \mathcal{G}_1 e^{i\boldsymbol{q}\cdot\boldsymbol{x}+\omega t}$, where $\mathcal{G} = \{\varphi, \xi_{1,2}\}$, the linearized system (1)-(5) yields the dispersion relation $\omega(q)$ in the form $\omega^2 + f_1(q)\omega + f_2(q) = 0$, where $f_{1,2}$ depend also on the physical parameters. The two roots of this quadratic equation describe two modes, $\omega_{1,2}(q)$. The presence of the Goldstone mode, $\omega_1(0) = 0$, indicates the translation symmetry of the problem. If $\omega_2(0) > 0$, the basic state of the oxide layer is unstable with respect to spatially uniform perturbations: the planar oxide layer will shrink or expand. If $\omega_2(0) < 0$, it can be shown that $\omega_2(q) < 0$ for all q and the oxide layer can become unstable only with respect to spatially periodic perturbations corresponding to $\omega_1(q) > 0$. The dispersion curve $\omega_1(q)$ is shown in fig. 2 by the dashed line. It is therefore the competition between the destabilizing effect of the electric-field–dependent chemical reactions and the stabilizing effect of the surface energy (dependence of the activation energy on the Laplace pressure) that determines the wavelength selection. We see that the most rapidly growing mode has, in this particular case, the wavelength $\lambda_{\max} \approx 300\,\mathrm{nm}$ which is in the range of typically observed values of the pore diameter and interpore spacing [3]. Near the instability threshold, one finds $\omega_1(q) = a_1 q^2 - a_2 q^4$, where $a_{1,2} > 0$ are functions of the physical parameters. For the interface perturbations, a multiple-scales analysis near the instability threshold yields $\tilde{\xi}_{1,2} = h(\boldsymbol{x}, t)$, where $h(\boldsymbol{x}, t)$ is governed by the Kuramoto-Sivashinsky (KS) equation, $h_t + a_1\nabla^2 h + a_2\nabla^4 h - \frac{v_s}{2}(\nabla h)^2 = 0$. Solutions of the KS equation are known to have the form of spatio-temporally chaotic cells, splitting and merging, and having well-defined average size [12]. In fact, spatially irregular porous structures are often observed during the anodization of aluminum [3], titanium [13] and tin [14]. However, in order to explain the formation of spatially regular, hexagonal arrays of pores, some additional mechanism is needed that would produce a *short-wave* instability.

We propose that the elastic stress dependence of the activation energy of the dissolution reactions at the oxide-electrolyte interface can damp the long-wave perturbations and yield a short-wave instability. The volume expansion due to the oxidation reaction creates stress resulting from the contact between the metal and the amorphous oxide with different intermolecular distances. Such stress can be modeled analogously to the stress in epitaxial crystalline films [15]. Thus we consider now $s_{ij}^{\pm} \neq 0$ in (6) and, in addition to (1)-(5), solve the equations of mechanical equilibrium, $\partial_j \sigma_{ij}^{m,o} = 0$, in both the metal substrate $-\infty < z < \xi_1$, and the oxide layer $\xi_1 < z < \xi_2$, denoted by the superscripts m and o, respectively. The boundary conditions are

$$
\begin{aligned}
z = \xi_1 : \qquad & \boldsymbol{u}^m = \boldsymbol{u}^o,\ \left(\sigma_{ij}^m - \sigma_{ij}^o\right) n_j^{(1)} = 0; \\
z = \xi_2 : \qquad & \sigma_{ij}^o n_j^{(2)} = 0;
\end{aligned}
$$

and $\boldsymbol{u}^m \to 0$ as $z \to -\infty$. Here $\boldsymbol{u}$ is the displacement vector, $n_j^{(1,2)}$ are the normal vectors of the metal-oxide and oxide-electrolyte interfaces, and σ_{ij} is the stress tensor, related to the strain tensor, $u_{ij} = (1/2)(\partial_i u_j + \partial_j u_i)$, by the following stress-strain relations in the metal and oxide [15,16]:

$$
\begin{aligned}
\sigma_{ij}^m &= 2\mu^m \left[u_{ij}^m + \left(\frac{\nu^m}{1 - 2\nu^m} \right) \delta_{ij} u_{kk}^m \right], \\
\sigma_{ij}^o &= 2\mu^o \left[u_{ij}^o + \left(\frac{\nu^o}{1 - 2\nu^o} \right) \delta_{ij} u_{kk}^o - \left(\frac{1 + \nu^o}{1 - 2\nu^o} \right) \eta \delta_{ij} \right].
\end{aligned}
$$

Here μ is the shear modulus, ν is the Poisson ratio, δ_{ij} is the Kronecker symbol, η is the metal-oxide misfit strain associated with the aluminum oxide volume expansion $\upsilon = (V^o - V^m)/V^m = 2\eta$, and the metal substrate is chosen as the reference state. The basic state

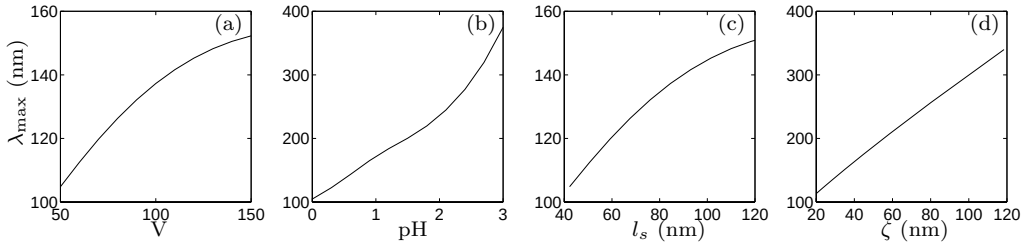

Fig. 3 – Dependence of the wavelength of the most rapidly growing mode above the instability threshold on (a) the applied voltage; (b) the electrolyte *p*H; (c) the basic state oxide thickness l_s. All other parameters are as given in the text. (d) shows the dependence of $\lambda_{\max}$ on the characteristic stress length, ζ, at the instability threshold (as computed in fig. 4).

solution of the elasticity problem is an undeformed metal substrate, $\boldsymbol{u}_0^m = \sigma_{ij}^m = 0$, supporting a strained planar oxide layer, $\boldsymbol{u}_0^o = (0, 0, zu_{zz}^o)$, where $u_{zz}^o = [(1+\nu^o)/(1-\nu^o)]\eta$ and the only nonzero components of the stress tensor are $\sigma_{xx}^o = \sigma_{yy}^o = -2\mu^o u_{zz}^o$. The basic state stress in the oxide renormalizes the kinetic coefficients $k_\pm$ in (6).

We now examine the stability of the basic state. Consider perturbations of the displacement fields, $\boldsymbol{u} - \boldsymbol{u}_0 = \boldsymbol{u}_1(z)e^{i\boldsymbol{q}\cdot\boldsymbol{x}+\omega t}$, linearize the elastic problem, and combine with the linearized system (1)-(5) to obtain the quadratic dispersion relation, $\omega^2 + g_1(q)\omega + g_2(q) = 0$, where g_1 and g_2 are functions of $s_{ij}^{\pm}$ and η, as well as the elastic constants and other physical parameters. Taking the typical parameter values mentioned above, as well as [17]: $\mu^m = 2.63\times10^{10}\,\mathrm{N\,m^{-2}}$, $\mu^o = 1.31\times10^{11}\,\mathrm{N\,m^{-2}}$, $\eta = 0.2$, $\nu^m = \nu^o = 0.33$, $\rho = 2.36\times10^{28}\,\mathrm{m^{-3}}$, $T = 373\,\mathrm{K}$, and estimating [7, 9]: $s_{xx}^+ = s_{yy}^+ = 1.02\times10^{-3}$, $s_{xx}^- = s_{yy}^- = -6.47\times10^{-4}$, $\gamma^+ = -7.88\,\mathrm{N\,m^{-1}}$, $\gamma^- = 7.22\,\mathrm{N\,m^{-1}}$, we find that one mode is stable, and the dispersion curve for the other mode is presented in fig. 2 by the solid line. The unstable mode yields a short-wave instability with the maximum growth rate at the wavelength $\lambda_{\max} \approx 100\,\mathrm{nm}$, which is consistent with experimental measurements of the pore diameter and interpore spacing [3]. The perturbations of the metal-oxide and oxide-electrolyte interfaces are in phase, also in agreement with experimental observations. Thus, the dependence of the interfacial kinetics on the elastic stress can damp the long-wave perturbations and shift the unstable mode from a long-wave instability with chaotic dynamics to a short-wave instability that occurs at a *nonzero* wavenumber. The wavenumber selection is the result of the competition between the destabilizing effect of the electrochemical reactions and the stabilizing effect of the elastic stress. It is important to note that the stabilizing effect of the elastic stress is always dominant for the long-wave modes and therefore the instability occurs only for a finite wave number. Such an instability is known to result in spatially regular hexagonal patterns [12].

Figure 3(a) shows the dependence of $\lambda_{\max}$ on the applied voltage above the instability threshold. The wavelength increase with the voltage is in accordance with experiments [1, 3, 5]. Figure 3(b) shows the increase of $\lambda_{\max}$ with the electrolyte *p*H, which is also confirmed by experimental measurements [5,6]. The scaling of $\lambda_{\max}$ with the basic state oxide thickness, l_s, and the characteristic stress length, $\zeta = vl_s$, is displayed in figs. 3(c) and (d), respectively. One can see that $\lambda_{\max}$ (pore diameter) increases with l_s that, in turn, increases with the applied voltage (see (8)). One can also see that $\lambda_{\max}$ almost linearly depends on the elastic stress length. Figure 4 presents a "phase diagram" in the plane of the applied voltage and volume expansion. We observe that the short-wave instability occurs in a rather limited range of the volume expansion. This agrees with experimental observations that the hexagonal ordering of pores occurs in a narrow range of the aluminum oxide volume expansion [8].

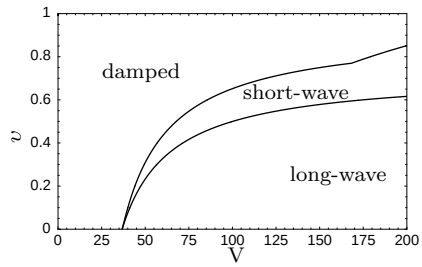

Fig. 4 – Phase diagram in the applied voltage and volume expansion. $s^+_{xx} = s^+_{yy} = 4.36 \times 10^{-4}$, $s^-_{xx} = s^-_{yy} = -2.76 \times 10^{-4}$, $\gamma^+ = -10.94\,\mathrm{N\,m^{-1}}$, $\gamma^- = 7.29\,\mathrm{N\,m^{-1}}$, and all other parameters are as given in the text.

In order to demonstrate the possibility of the formation of hexagonal pore arrays, we numerically solve the following model nonlinear evolution equations for the positions of the interfaces $\xi_{1,2}$:

$$\partial_t \xi_1 = L_{11}\xi_1 + L_{12}\xi_2 + \psi_1(\xi_1 - \xi_2), \tag{9}$$

$$\partial_t \xi_2 = L_{21}\xi_1 + L_{22}\xi_2 + \psi_2(\xi_1 - \xi_2). \tag{10}$$

Here L_{ij} are integro-differential operators derived from the linear stability problem, such that the corresponding Fourier transforms, $\hat{L}_{ij}(q)$, are the components of the linear evolution matrix in Fourier space that are related to the coefficients of the dispersion relation by $\hat{L}_{11} + \hat{L}_{22} = -g_1(q)$, $\hat{L}_{11}\hat{L}_{22} - \hat{L}_{12}\hat{L}_{21} = g_2(q)$, and the functions $\psi_{1,2}$ represent nonlinearities. Due to the translation invariance, the functions $\psi_{1,2}$ depend on $\xi_1 - \xi_2$ and are chosen to be in the generic polynomial form $\psi_{1,2} = \alpha_{1,2}(\xi_1 - \xi_2)^2 + \beta_{1,2}(\xi_1 - \xi_2)^3$.

A selected result of the numerical solution of the system (9)-(10) by a pseudospectral method, with small random noise initial conditions, is given in fig. 5. After some transient behavior the pattern evolves toward a hexagonal lattice, see fig. 5. The lattice initially contains many defects that slowly anneal. As in experiment, the interfaces are in phase, and the modulation of the oxide-electrolyte interface is always larger than that of the metal-oxide interface.

In conclusion, we have developed a theory of the formation of pore arrays during anodization of aluminum. We have shown that the strong dependence of the electric current on the overpotential leads to the instability of a planar oxide layer that, in combination with the

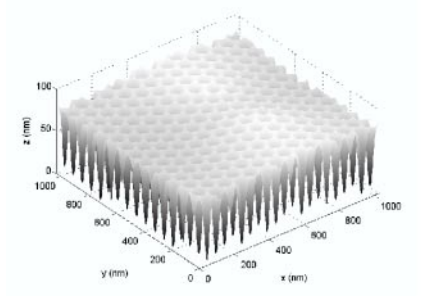

Fig. 5 – Gray-scale representation of the height of the oxide-electrolyte interface for the typical parameter values.

dependence of the activation energy on the Laplace pressure, yields the wavelength selection. The instability is long wave in this case, and near the threshold it is described by the KS equation whose solutions exhibit spatio-temporal chaos. This mechanism can explain the formation of irregular arrays of pores in alumina, as well as in the oxides of other valve metals produced by anodization. The spontaneous ordering of pores in hexagonal arrays is attributed to the change of the instability type from long wave (with zero wave number at threshold) to short wave (with nonzero wave number at threshold); the latter is known to produce hexagonal patterns due to the resonant quadratic interaction between unstable modes [12]. The transition from the long-wave to short-wave instability is caused by the effect of elastic stress that damps the long-wave perturbations. Note that our analysis is weakly nonlinear, while the deep pores cannot be treated as small perturbations of planar interfaces. Fully nonlinear treatment will be necessary to describe the growth of deep pores.

* * *

We thank Z. Xiao, Y. Tolmachev and H. Wang for stimulating discussions. GKS and AAG acknowledge the support of the NSF grant #DMS-0204643. GKS also acknowledges the support of the NSF IGERT Fellowship. ISA and VMV are supported by the US DOE, grant W-31-109-ENG-38.

REFERENCES

[1] Paolini G. *et al.*, *J. Electrochem. Soc.*, **112** (1965) 32; O'Sullivan J. P. and Wood G. C., *Proc. Roy. Soc. London, Ser. A.*, **317** (1970) 511.
[2] Bandyopadhyay S. *et al.*, *Nanotechnology*, **7** (1996) 360.
[3] Li F., Zhang L. and Metzger R. M., *Chem. Mater.*, **10** (1998) 2470; Jessensky O., Müller M. and Gösele U., *Appl. Phys. Lett.*, **72** (1998) 1173.
[4] Masuda H. and Fukuda K., *Science*, **268** (1995) 1466; Masuda H. *et al.*, *Appl. Phys. Lett.*, **71** (1997) 2770; Thompson G. E., *Thin Solid Films*, **297** (1997) 192; Huczko A., *Appl. Phys. A*, **70** (2000) 365; Sun M. *et al.*, *Appl. Phys. Lett.*, **78** (2001) 2964; Schmid G., *J. Mater. Chem.*, **12** (2002) 1231; Cheng G. and Moskivits M., *Adv. Mater.*, **14** (2002) 1567; Choi J. *et al.*, *J. Appl. Phys.*, **94** (2003) 4757.
[5] Parkhutik V. P. and Shershulsky V. I., *J. Phys. D*, **25** (1992) 1258.
[6] Thamida S. K. and Chang H.-C., *Chaos*, **12** (2002) 240.
[7] Valance A., *Phys. Rev. B*, **52** (1995) 8323; Guo W. and Johnson D., **67** (2003) 075411.
[8] Li A. P. *et al.*, *J. Appl. Phys.*, **84** (1998) 6023; Nielsch K. *et al.*, *Nano Lett.*, **2** (2002) 677.
[9] Grinstein G., Tu. Y. and Tersoff J., *Phys. Rev. Lett.*, **81** (1998) 2490; Barvosa-Carter W. *et al.*, **81** (1998) 1445.
[10] Diggle J. W. (Editor), *Oxides and Anodic Films*, Vol. **2** (Marcel Dekker, New York) 1973.
[11] Bockris J. O'M. and Reddy A. K. N., *Modern Electrochemistry*, Vol. **2** (Plenum Press, New York) 1970.
[12] Cross M. C. and Hohenberg P. C., *Rev. Mod. Phys.*, **65** (1993) 851.
[13] Gong D. *et al.*, *J. Mater. Res.*, **16** (2001) 3331; Beranek R., Hildebrand H. and Schmuki P., *Electrochem. Solid-State Lett.*, **6** (2003) B12.
[14] Shin H.-C., Dong J. and Liu M., *Adv. Mater.*, **16** (2004) 237.
[15] Spencer B. J., Voorhees P. W. and Davis S. H., *Phys. Rev. Lett.*, **67** (1991) 3696; *J. Appl. Phys.*, **73** (1993) 4955.
[16] Landau L. D. and Lifshitz E. M., *Elasticity Theory* (Pergamon Press, Oxford) 1964.
[17] Schackelford J. F. and Alexander W. (Editors), *CRC Materials Science and Engineering Handbook*, 3rd edition (CRC Press, Boca Raton) 2001.